### **Computation & theory**



# Grain boundary migration facilitated by phase transformation and twinning in face-centered cubic metals

Bin Li<sup>1,\*</sup>, and Kefan Chen<sup>1</sup>

Received: 23 January 2023 Accepted: 16 August 2023 Published online: 28 September 2023

© The Author(s), under exclusive licence to Springer Science+Business Media, LLC, part of Springer Nature, 2023

### **ABSTRACT**

Migration of symmetric tilt grain boundaries (STGBs) in face-centered cubic (FCC) metals under shear loading is investigated in this work. The STGBs have a tilt axis of [110], and the angle  $\theta$  between the (111) invariant planes ranges from 8° up to 28° with a 2° increment. Interesting phase transformation and twinning are observed during GB migration in Cu, Ni but not in Al. The results show that for low values of  $\theta$ , under shear loading, a hexagonal close-packed (HCP) phase is formed along the original GB and the HCP phase grows via shear coupling of one of the two interfaces between the HCP and the FCC grain. As  $\theta$  increases, both interfaces between the HCP and the grains become mobile and the HCP region traverses and transforms the lattice of one grain into the other. Thus, shear coupling is accomplished and facilitated through FCC  $\rightarrow$  HCP  $\rightarrow$  FCC phase transformations. As  $\theta$  further increases to 18° and greater, instead of FCC  $\rightarrow$  HCP phase transformation, a {111} twin is formed along the original GB. The twin expands via shear coupling of the new GB between the twin and the FCC grain. Lattice correspondences are carefully analyzed for the phase transformation and twinning. The analyses indicate that the mobility of GBs is predominantly determined by how readily lattice transformation can be accomplished. The lattice correspondence in HCP twinning modes provide key insight on the observed GB migration behavior.

### Introduction

When an external shear strain is applied parallel to a grain boundary (GB), how the GB responds to the shear strain has been an interesting problem that is of great significance in physical metallurgy. The shear strain may drive the GB into motion via shear coupling

or sliding or both [1]. Shear coupling is referred to the coupled motion of a GB simultaneously in the GB normal direction and in parallel to the GB plane and has been observed in experiments and atomistic simulations [1–9]. The coupling factor  $\beta$  is defined as  $\beta = \frac{v_{\parallel}}{v_{\perp}}$  [1], where  $v_{\parallel}$  is the lateral velocity component parallel to the GB plane, and  $v_{\perp}$  the velocity component along

Handling Editor: N. Ravishankar.

Address correspondence to E-mail: binl@iastate.edu



<sup>&</sup>lt;sup>1</sup> Department of Chemical and Materials Engineering, University of Nevada, Reno, NV 89557, USA

the GB normal. In their pioneering work, Cahn et al. [1] showed that some coincidence site lattice (CSL [10]) GBs in face-centered cubic (FCC) copper (Cu) with [001] tilt axis migrated via shear coupling when an external shear strain was applied parallel to the GB plane. They observed two branches of coupling factor: One corresponds to the (100) invariant plane, and the other to the (110) invariant plane. These invariant planes are very similar to the second invariant planes defined in classical twinning theory [11, 12]. During GB migration via shear coupling, atoms on the invariant plane of one grain are homogenously sheared to the corresponding plane which is the crystallographically equivalent plane of the neighboring grain. In other words, no distortion should happen to the invariant plane during GB migration. The acute angle  $\theta$ between the invariant planes of the neighboring grains can be used to define  $\beta = 2\tan\frac{\theta}{2}$  [1]. Note that this definition is essentially the same as the definition of "magnitude of twinning shear" in the classical twinning theory. The similarity between GB shear coupling and deformation twinning was noted by a number of researchers in terms of invariant planes and the magnitude of shear [6, 9].

Recently, Li and Leung [13] showed that in shear coupling, the choice of the invariant plane generally follows the rules of the classical twinning theory. The active invariant plane should be a low-index plane with highest atom density such that the number of atoms that are directly sheared to the lattice of neighboring grain is maximal, and accordingly, the atomic shuffles involved in the lattice transformation is relatively simple. For example, for CSL GBs with [001] tilt axis, it was found that the invariant plane alternated between the two low-index planes (100) and (110) as the misorientation angle varied [1]. From the literature data of GB migration kinetics via shear coupling, it can be seen that the value of  $\theta$ , which determines the magnitude of shear, is directly correlated with the migration velocity of GBs via shear coupling. For a specific invariant plane, smaller values of  $\theta$  always give rise to faster migration velocities, irrespective of GB coherency, structure and energy. Immediately, it follows that for those symmetric tilt GBs (STGBs) with boundary plane not far away from the close-packed plane, i.e., {111} plane of FCC metals, their mobility via shear coupling should be very low. This brings up an interesting question: How those STGBs with (110) tilt axis and {111} invariant planes migrate under shear loading?

Kinetics of shear coupling of STGBs in the [110]-[110]-[001] orientations with (110) tilt axis in Ni was systematically studied by Homer et al. using synthetic driving force approach [14]. Shear response of  $\Sigma 9\langle 110\rangle \{221\}$  and  $\Sigma 11\langle 110\rangle \{131\}$  STGB in FCC metals was also investigated by Wan and Wang [15, 16]. In this work, we present interesting simulation results of shear coupling of GBs over a range of value of  $\theta$  in the [110]-[111]-[112] orientation with [110] tilt axis in FCC metals Cu, Ni and Al. Novel analyses of structural evolution, especially lattice correspondences, are conducted to reveal the mechanisms for GB motion. Phase transformation and twinning are activated at the GBs under shear loading and facilitate GB migration via shear coupling. The results obtained provide new insight on the physics of GB migration and mobility.

### Simulation method

Grain boundaries with [110] tilt axis are constructed based on the STGB model. A bi-crystal model in our simulations is shown in Fig. 1. From the previous work [13], the GB motion mode, i.e., shear coupling or sliding, is directly determined by the angle  $\theta$  between the invariant planes of the two grains. The tilt angle  $\phi$ , which is the angle between the (111) planes of the two grains, is not a convenient structural parameter to describe GB motion or mobility. This is because for rotation axes such as [001] and [110], more than one invariant plane may be present as the tilt angle  $\phi$  varies. For the (111) invariant plane,  $\theta$  is related to  $\phi$  by:  $\phi = 39^{\circ} - \theta$ . On the other hand, no matter how the value of  $\phi$  changes, mode of motion is always directly related to  $\theta$  which is the angle between the active invariant planes of two neighboring grains and uniquely defines the magnitude of shear s. To investigate how s influences the motion of the STGBs with [110] tilt axis,  $\theta$  is chosen from 8°, 10°,..., up to 28°, at an interval of  $2^{\circ}$ . After relaxation, the actual values of  $\theta$ may slightly deviate from the chosen values, but such deviation is not expected to affect the overall trend and the conclusions drawn from the results. We also find that, as  $\theta$  further increases, the invariant plane shifts from the (111) to another plane and details of GB motion for those larger values of  $\theta$  will be presented elsewhere.



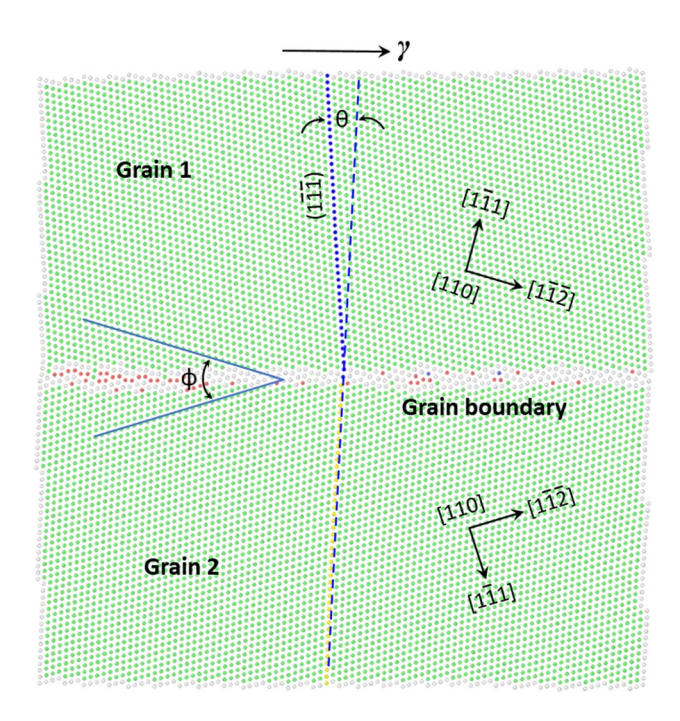


**Figure 1** Initial bi-crystal that forms a symmetric tilt grain boundary in FCC Cu. The rotation axis is [110]. One of the (111) planes of the top grain is preselected and highlighted in blue. This plane is the invariant plane during GB migration. Common neighbor analysis is used to distinguish crystal structures. The angle  $\theta$  between the invariant planes of the two crystals is a key parameter that describes the characteristics of GB motion.  $\phi$  is the angle between the (111) planes of the bi-crystal, or the tilt angle, and  $\phi = 39^{\circ} - \theta$ .

First, we construct two identical single crystals but the misorientation angle between them is chosen such that  $\theta$  equals the preselected values. Then the two single crystals are bonded together, followed by relaxation to form a STGB. The system size is about 680000 atoms, with dimensions of 20 nm  $\times$  20 nm  $\times$ 20 nm. Embedded atom method (EAM) [17, 18] type of interatomic potentials for Cu [19], Ni [20] and Al [20] is used for our simulations. The simulation temperature is fixed at 100 K by using the Nosé-Hoover thermostat [21, 22]. This temperature is chosen so as to reduce thermal noise in structural analyses. The simulation results are similar when the temperature is set at 300 K. To generate GB migration via shear coupling, a shear strain is created by displacing the atoms on the top surface of the system at a constant rate (0.02 Å/ps) while those atoms on the bottom surface are fixed. The shear strain rate is about  $1.0 \times 10^8$ /sec. The time step size equals 1.0 fs. The system is relaxed for 50 ps before the shear loading is applied. Large-scale atomic/molecular massively parallel simulation (LAMMPS) package [23] is used for the simulations. OVITO [24], which provides functions for structural visualization and analyses, is used to analyze the structural evolution during GB migration.

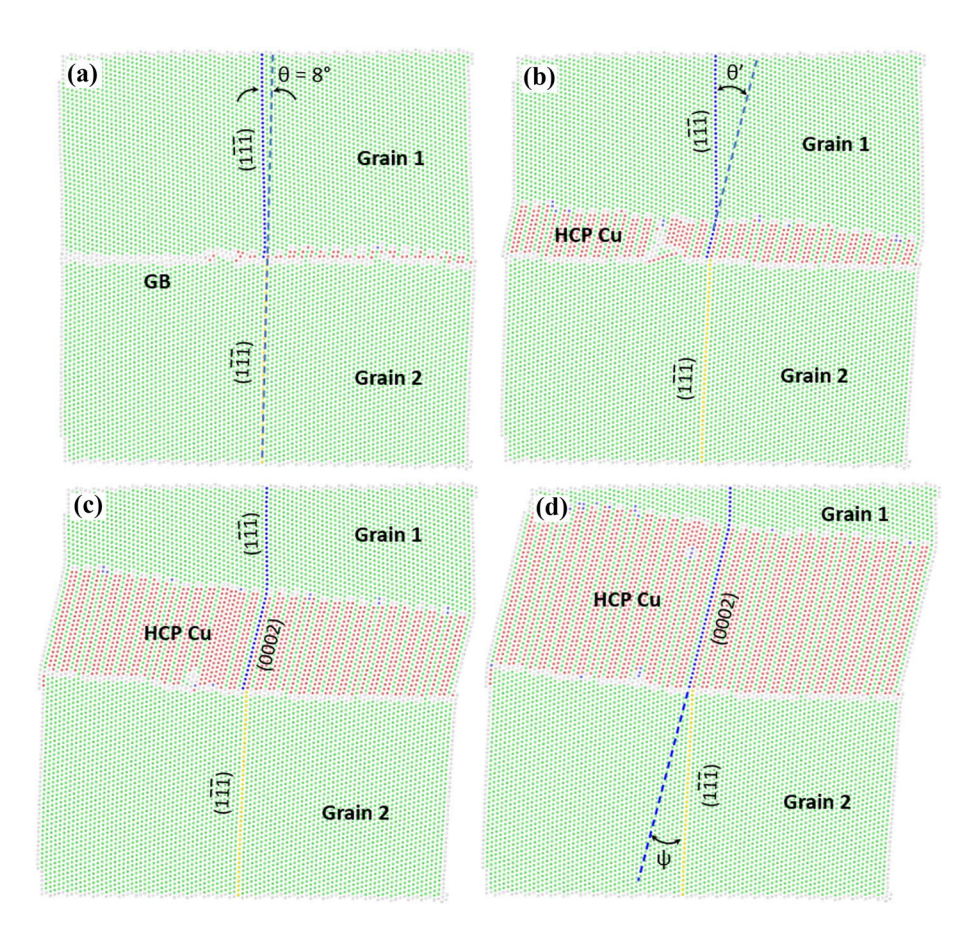
In our simulations, no periodic boundary condition is applied along any dimension. In periodic boundary condition, atoms on the opposite boundaries interact. If the simulated lattice system lacks a well-defined periodicity in that crystal orientation, interatomic interaction on these boundaries would differ from the interaction between bulk atoms. Thus, unintended and undesirable internal stresses would be present in the system and spurious structures might be created by such internal stresses.

### Results

We present our simulation results starting with the low values of  $\theta$ . Only the results for Cu are presented in the main text, and the results for Ni and Al are presented in Supplemental Material. Figure 2a shows the relaxed GB when  $\theta$  = 8°. Common neighbor analysis (CNA) [25] is used to distinguish different crystal structures. In this color scheme, the FCC is displayed in green, the HCP is displayed in red, whereas atoms on the free surfaces and interfaces are displayed in white. In this plot, the (111) planes of Grain 1 and Grain 2 are preselected and colored in blue and yellow and this color pattern is retained throughout the simulation. Thus, these planes, also the invariant planes, serve as marker lines that help track the evolution of the GB during simulation. Interestingly, after relaxation, some atoms on the GB are already recognized as in HCP in OVITO, which actually has a faulted structure as analyzed in the following. This relaxed structure is similar to the report by Rittner et al. [26] in which narrow stacking faults (SFs) were identified after relaxation. As the shear strain increases, surprisingly, a region of hexagonal close-packed (HCP) Cu is formed along the original GB. The formation of the HCP creates two new interfaces or GBs between the FCC and the HCP structures (Fig. 2b). Note that these red atoms are not on either of the two {111} planes of Grain 1, and thus they are not formed by Shockley partial dislocations. The HCP phase grows into Grain 1 as the top GB migrates upward. At this time, the bottom GB remains almost still. Note that the HCP structure



Figure 2 a Relaxed GB when  $\theta = 8^{\circ}$ . The  $(1\overline{11})$ planes of the bi-crystal are preselected and highlighted in blue and yellow. b Under the shear strain, a band of HCP Cu is forming along the GB and grows into Grain 1. The HCP phase is displayed in red in common neighbor analysis. c The HCP phase keeps growing at the expense of Grain 1. Note that the (111) plane is transformed into the (0002) basal plane of the HCP. d Most of Grain 1 is transformed into the HCP.  $\psi \approx 11.5^{\circ}$ , which is the angle between the (0002) of the HCP and the  $(1\overline{11})$  of Grain



has a high density of SFs on the (0002) basal plane (Fig. 2c). The property of these SFs will be analyzed below. As the shear strain further increases, the HCP region expands at the expense of Grain 1. Meanwhile, the bottom GB slightly moves away from the horizontal position and migrates upward (Fig. 2d). Now, if we treat the HCP as a new grain, two pairs of corresponding invariant planes can be defined: the (111) plane of Grain 1 and the (0002) of the HCP, and the (111) plane of Grain 2 and the (0002) plane of the HCP. (The angle between them is denoted by  $\psi$ .) Note that  $\psi \neq \theta$ , and  $\psi \approx 11.5^{\circ}$  in this particular case. The lattice transformation can be described as:

$$(1\overline{11})_{\text{grain }1} \rightarrow (0002)_{\text{HCP}}$$

As  $\theta$  is increased to 10° (Fig. 3a), similar FCC  $\rightarrow$  HCP phase transformation is observed. Figure 3a shows the initial relaxed GB when  $\theta$  = 10°. Under the shear strain, an HCP phase is formed between the two FCC grains. This HCP region grows at the expense of Grain 1. It can also be seen that

the density of basal stacking faults decreases as  $\theta$  increases. Note that as  $\theta$  increases, the value of angle  $\psi$  decreases, and this will affect the mobility of the bottom interface between the HCP and Grain 2. The lattice transformation can also be described as:

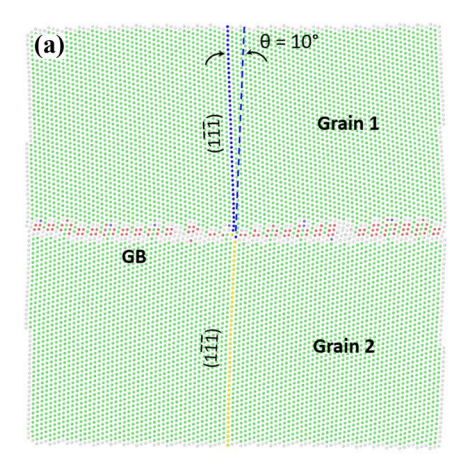
$$(1\overline{11})_{\text{grain }1} \rightarrow (0002)_{\text{HCP}}$$

As  $\theta$  is further increased to 12°, not only the top interface, but the bottom interface between the FCC and the HCP is also mobile. Figure 4a displays the relaxed GB when  $\theta$  = 12°. As the shear strain increases, an HCP region is formed along the GB. However, a different scenario can be seen. The bottom interface is also moving upward. As a result, as the HCP region is moving upward and consuming Grain 1, the HCP phase is also transforming back into FCC that is becoming part of Grain 2. The lattice transformation in this scenario can be described as:

$$(1\overline{11})_{\text{grain }1} \to (0002)_{\text{HCP}} \to (1\overline{11})_{\text{grain }2}$$



**Figure 3 a** Relaxed GB when  $\theta = 10^{\circ}$ . **b** Under the shear strain, an HCP phase is formed and grows at the expense of Grain 1. Again, the lattice transformation is such that the  $(1\overline{11})$  of Grain 1 is transformed into the (0002) basal plane of the HCP.  $\psi \approx 10.6^{\circ}$ .



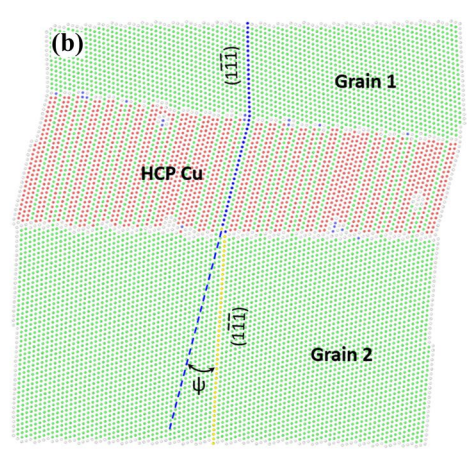
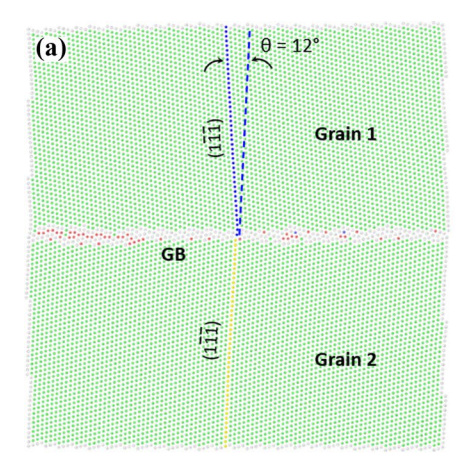
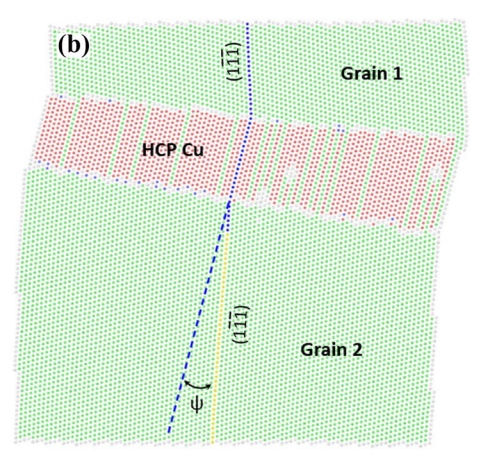


Figure 4 a Relaxed GB when  $\theta = 12^{\circ}$ . b Under the shear strain, an HCP phase is formed and grows into Grain 1. But interestingly, the two interfaces or GBs between the FCC and HCP are both moving upward. The (111) of Grain 1 is transformed into the (0002) basal plane of the HCP, and the latter is transformed into the (111) of Grain 2.  $\psi \approx 9.8^{\circ}$ .





As  $\theta$  is further increased to a larger value of 14° (Fig. 5a), a different behavior is observed. Under the shear strain, the HCP phase evolves into a thin strip and the whole region moves upward, transforming Grain 1 into Grain 2 (Fig. 5b and c). This indicates that the top and the bottom interface between the HCP and the FCC have close mobility and both migrate upward at similar velocities. Eventually, most of Grain 1 is transformed into Grain 2. The lattice transformation can also be described as:

$$(1\overline{11})_{\text{grain }1} \rightarrow (0002)_{\text{HCP}} \rightarrow (1\overline{11})_{\text{grain }2}$$

When  $\theta$  is increased to 16° (Fig. 6a), the top interface between the HCP and Grain 1 has the highest migration velocity. The bottom interface also has finite mobility but migrates slower than the top interface, leading to a wide HCP region. Some part of the HCP has a low density of basal SFs.

Further increase of  $\theta$  to 18° (Fig. 7a) results in an interesting transition in the GB motion. Twinning occurs at the GBs. As the shear strain increases, initially, the GB evolves into a thin strip of an HCP structure that moves upward. The lattice of Grain 1 is transformed into the lattice of Grain 2, as seen from the deflected blue trace of (111). Some blue atoms of the (111) in Grain 1 are aligned to the (111) of Grain 2 (Fig. 7b). Surprisingly, as the shear strain further increases, the HCP strip stops moving upward, instead, a thin layer of FCC twin is formed along the top interface between Grain 1 and the HCP (Fig. 7c). The twinning plane is exactly the (111) of Grain 1. The twinned region separates the HCP strip from Grain 1, and the HCP strip reverses it migration direction from upward to downward. As the HCP strip moves downward, the twinned region expands at the expense of Grain 2. Obviously, the twin growth has nothing to do with Shockley partial dislocations that glide on twin boundaries (TB) and mediate twin growth in FCC metals in classical twinning.



Figure 5 a Relaxed GB when  $\theta$ = 14°. b Under the shear strain, the initial GB evolves into a narrow zone of HCP structure which moves into Grain 1. c As the HCP strip moves upward, the (111) of Grain 1 is transformed into the (111) of Grain 2. d As the HCP zone moves upward, most of Grain 1 is consumed as a result of the migration of the two interfaces between the FCC and the HCP.  $\psi \approx 8.3^{\circ}$ .

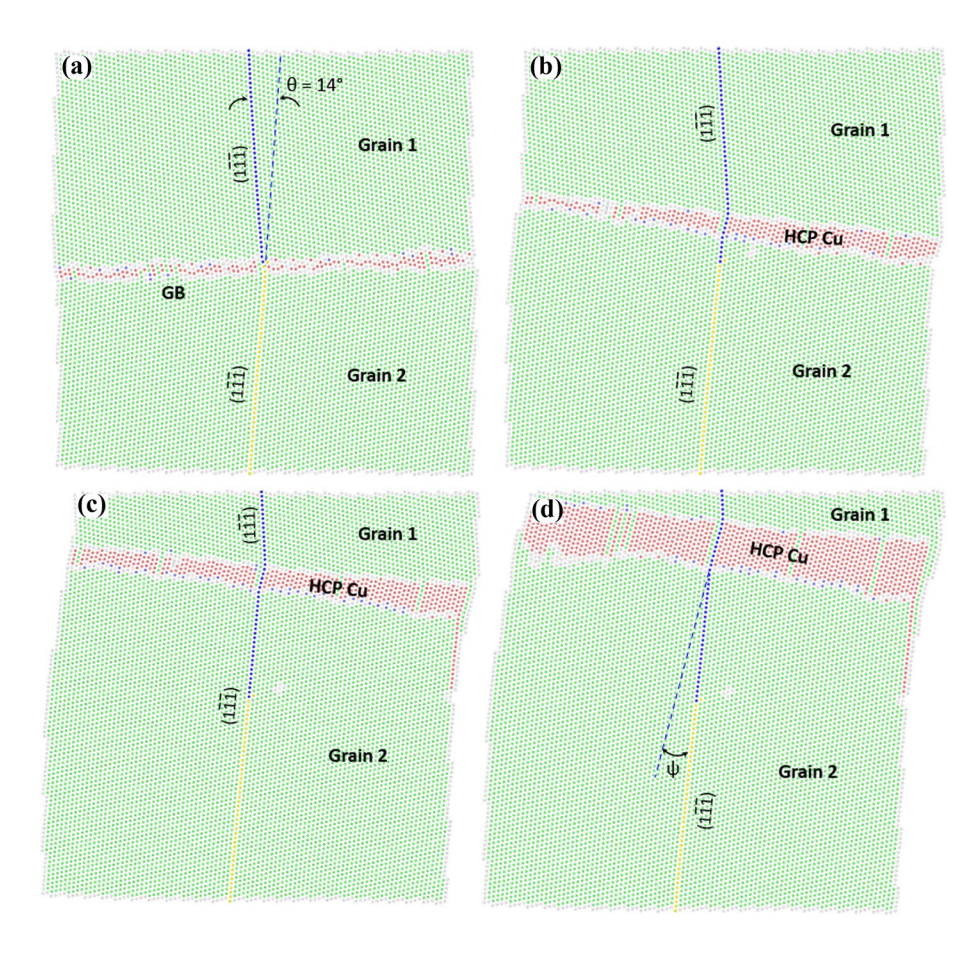
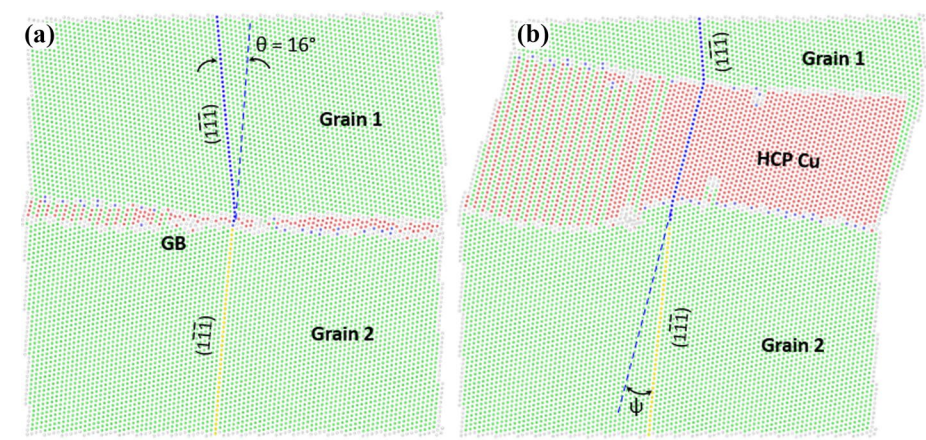


Figure 6 a Relaxed GB when  $\theta = 16^{\circ}$ . b As the shear strain increases, an HCP phase is formed and consumes Grain 1. The top GB migrates faster than does the bottom GB, so the HCP region expands.  $\psi \approx 8.1^{\circ}$ .

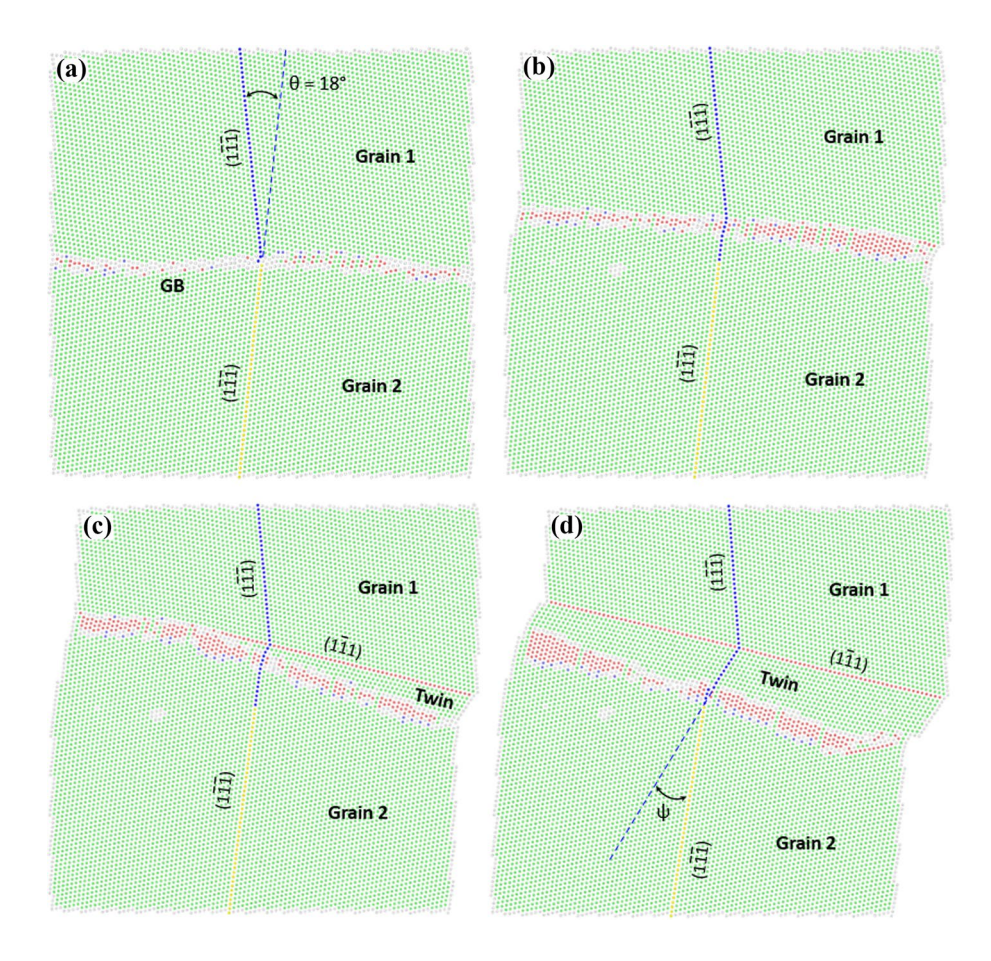


Similar twin formation between a migrating GB and an FCC matrix is observed in all other values of  $\theta$ , i.e.,  $20^{\circ}$ ,...,  $28^{\circ}$ . For comparison, we only present the results from  $\theta = 28^{\circ}$ . Figure 8a shows the relaxed GB in common neighbor analysis. For this large value of  $\theta$ , the GB does not move upward as the shear strain increases, instead, an FCC twin is formed and grows between the GB and Grain 1 (Fig. 8b). For clarity, a

magnified view of the twinned region is shown in Fig. 8c. It can be seen that, as the twin is formed, not through the glide of twinning dislocations because the twin boundary remains still, the blue (111) of Grain 1 is transformed into the (111) of the twin, and then the yellow (111) of Grain 2 is transformed into the (111) of the twin through the downward migration of the GB which has been rotated.



Figure 7 a Relaxed GB when  $\theta = 18^{\circ}$ . **b** As the shear strain increases, at first the GB migrates upward. **c** Then, a twin structure is formed along the moving GB. **d** The twinned region expands as the thin HCP region changes the migration direction to downward.  $\psi \approx 22^{\circ}$ .



Simulations on STGBs with [110] tilt axis in Ni show very similar behavior to that in Cu (see Fig. S1 and S2 in Supplemental Material). For small values of  $\theta$ , FCC  $\rightarrow$  HCP transformation occurs at the GBs. Further increase of  $\theta$  leads to twin formation at the GBs. In sharp contrast, no FCC  $\rightarrow$  HCP phase transformation and twinning are observed in Al, irrespective of the value of  $\theta$ , and only GB sliding is observed (Fig. S3).

### **Analysis and discussion**

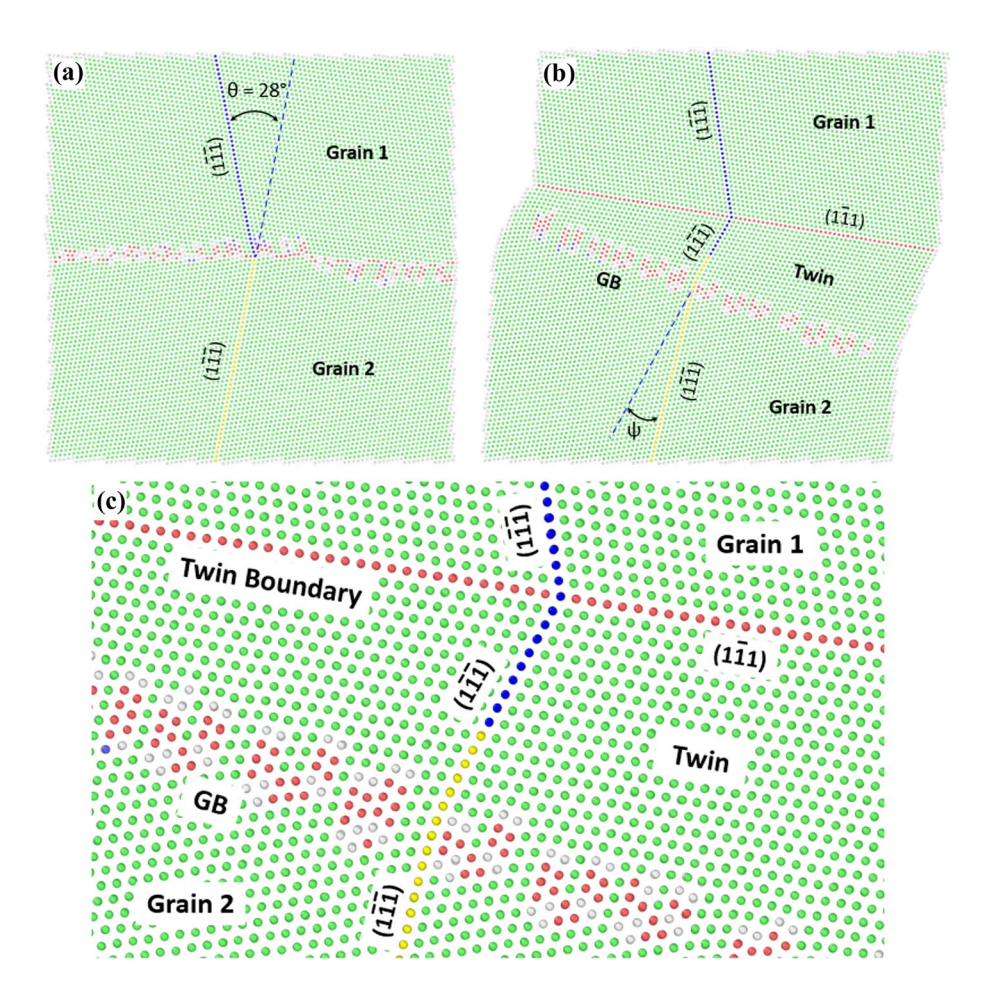
## Lattice correspondence analysis in the FCC $\rightarrow$ HCP $\rightarrow$ FCC phase transformations

Our simulation results reveal interesting FCC → HCP phase transformation and twinning at STGBs with [110] tilt axis in FCC Cu and Ni. The phase transformation and twinning facilitate GB shear coupling. These results bring up a crucially important feature in GB migration, that is, GB mobility is dominated by

how readily the lattice of a grain can be transformed into the lattice of the neighboring grain. If no phase transformation or twinning occurs, the mobility of GBs can be described by a single structural parameter  $\theta$ . In general, smaller values of  $\theta$  give rise to faster migration velocities or higher GB mobility [1, 13, 14]. For the STGBs with [110] tilt axis and (111) being the invariant plane, the GB plane is not far away from the close-packed plane (111) (Figs. 1, 2, 3, 4, 5, 6, 7, 8), and lattice transformation for these close-packed planes could be difficult via direct shear coupling. This is because the corresponding plane in the other grain may be irrational or more than one non-close-packed, high-index planes need to be combined to accomplish the lattice correspondence (see analysis below). When phase transformation or twinning occurs at the GBs, such a structural change makes the lattice transformation from one grain into the other much easier and thus facilitates GB migration via shear coupling, because lattice correspondence also exists in GB shear coupling [13]. From Fig. 2b, after the HCP phase is formed, the invariant planes between Grain 1 and the



**Figure 8** a Relaxed GB when  $\theta$  is further increased to 28°. **b** Under the shear strain, a twin is formed with respect to Grain 1. The GB is now migrating downward, leading to the growth of the twin. **c** A magnified view of the twin, twin boundary and GB. Due to the formation of the twin, the invariant plane has shifted to the (111) of the twin, leading to the change in migration direction of the GB.  $\psi \approx 12^{\circ}$ .



HCP becomes the  $(\overline{111})_{FCC}$  and  $(0002)_{HCP}$ . The new angle between these two invariant planes  $\theta'$  becomes actually larger than the initial  $\theta$ , and  $\theta'$  increases with increasing  $\theta$ . If we only consider the value of  $\theta$  which determines the magnitude of shear s, the FCC  $\rightarrow$  HCP transformation is not favorable because a larger s corresponds to a lower GB mobility [13]. However, the special structure of the new interface between Grain 1 and the HCP renders these interfaces with high mobilities.

The concept of "lattice correspondence" or "lattice transformation" in the solid-state phase transformation and deformation twinning was well stated by Christian [27]: "A deformation which is physically significant implies a one to one correspondence between vectors in the two lattices. Each vector in one lattice may be associated unambiguously with a 'corresponding' vector of the other lattice into which it is converted by the transformation." A key implication of this statement is that a crystallographic plane of one lattice must be transformed to its corresponding plane of the other lattice. In other words, atoms on a

crystallographic plane of the parent lattice must reside on its corresponding plane of the product lattice after the interface (a GB, TB or interphase boundary) connecting the two lattices migrates progressively into the parent. This requires that the displacements of individual atoms are a small fraction of the lattice parameter. Mathematically, such a lattice correspondence, which is a linear transformation, can be described by a second rank tensor [28]. In the following we show that, for the STGBs with [110] tilt axis and (111) being the invariant plane, phase transformation and twinning at the GBs do facilitate GB shear coupling, despite the increase in  $\theta'$ . The analyses of the lattice transformations involved in the FCC  $\rightarrow$  HCP phase transformation and in the twinning are presented below.

First, we analyze the lattice correspondence in the FCC  $\rightarrow$  HCP  $\rightarrow$  FCC transformations involved in the low values of  $\theta$  where no twinning occurs. From the simulation results (Figs. 2, 3, 4, 5, 6), it can be seen that, after the HCP is formed along the GB, two new interfaces are created between the FCC and the HCP. The top interface always has a good mobility. To



demonstrate how lattice correspondence analysis is conducted, we take  $\theta = 16^{\circ}$  as an example. Because the FCC and HCP are both close-packed structures, it is of interest to examine how the close-packed plane in the FCC is transformed to its corresponding plane in the HCP. First, we preselect a (111) plane of Grain 1 at an early time step before the HCP traverses through, and "dye" the atoms on this plane in blue (Fig. 9a). After the HCP grows and consumes Grain 1, the blue atoms are now in the HCP lattice (Fig. 9b). It can be readily seen that the preselected blue atoms are now residing on the {1100}, i.e., the prismatic plane of the HCP. Thus, the lattice correspondence in the FCC  $\rightarrow$  HCP phase transformation can be described as:

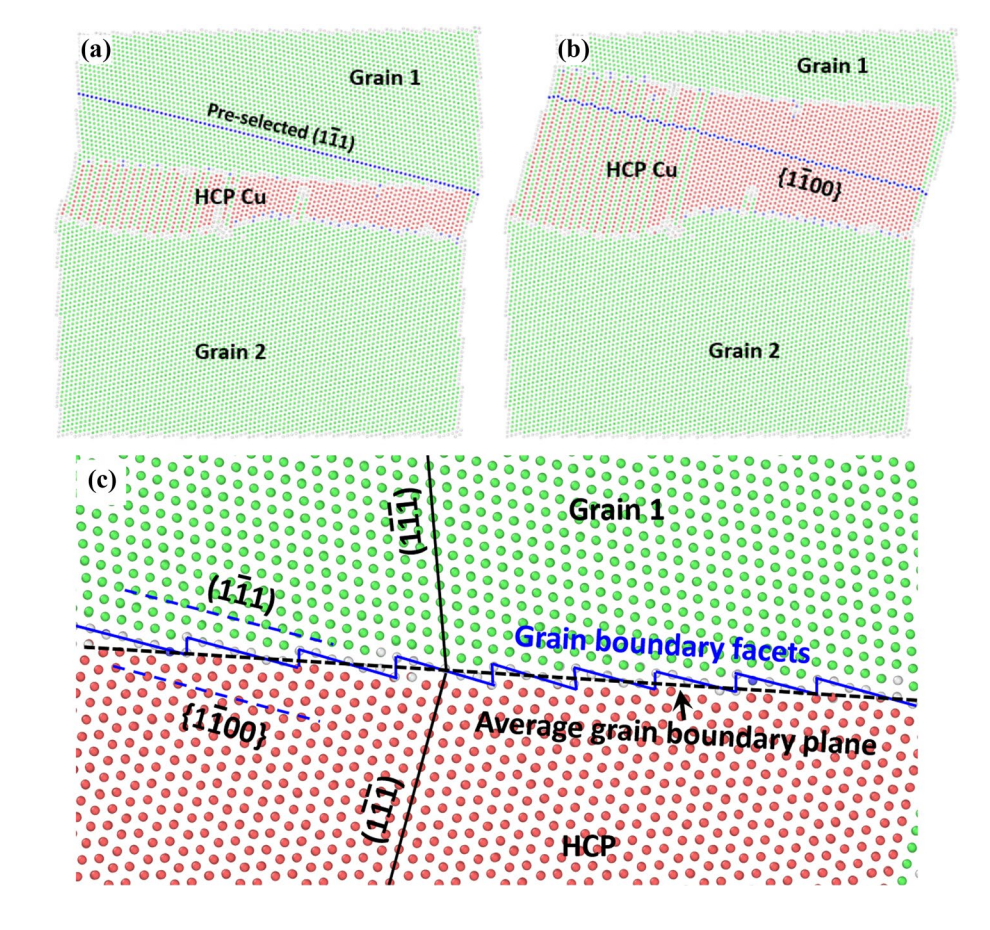
$$(1\overline{1}1)_{FCC} \rightarrow \{1\overline{1}00\}_{HCP}$$

To understand how this lattice transformation is accomplished, a magnified view of the top interface is shown in Fig. 9c. It is now clear that the top interface is composed of a series of small facets (on the order of

one to two nanometers). The crystallographic plane of these facets falls exactly between the (111) of FCC and the  $\{1100\}$  of HCP, i.e., the facets are the interfaces between the  $(111)_{FCC}$  and the  $\{1100\}_{HCP}$ . The traces of  $(111)_{FCC}$  and  $\{1100\}_{HCP}$  are denoted by the dashed blue lines. Another interesting behavior can also be seen—if the HCP is treated as a new grain, the average GB plane (denoted by the dashed black line) falls on the position that bisects the obtuse angle between the (1111) invariant planes of the FCC and the HCP.

The above analysis indicates that there must be a very easy pathway for the (111) of Grain 1 to be transformed into the  $\{1100\}$  of HCP. Figure 10a compares the structure of  $\{1100\}_{HCP}$ . Seven atoms are taken out of the preselected blue (111) plane in Fig. 9a. After the (111)<sub>FCC</sub> is transformed to the  $\{1100\}_{HCP}$ , the structures of the two planes are compared. The viewing direction of these plots is along the normal to the  $\{1110\}_{FCC}$  plane. It can be seen that the structure of  $\{1110\}_{FCC}$  and the structure of  $\{1110\}_{HCP}$ , when viewed along their normal direction, are very close with only minor differences

Figure 9 Lattice correspondence analysis in FCC → HCP phase transformation ( $\theta = 16^{\circ}$ ). a A (111) plane of Grain 1 is preselected and highlighted in blue. **b** As the HCP phase grows into Grain 1, the preselected (111) plane is transformed into the  $\{1\overline{1}00\}$  plane, i.e., the prismatic plane of the HCP phase. c Magnified view of the top interface between the FCC and HCP. The interface consists of multiple small facets that are  $(111)_{FCC} \parallel \{1100\}_{HCP}$ . If the HCP is treated as a new grain, the average GB plane approximately bisects the obtuse angle between the (111) invariant planes.





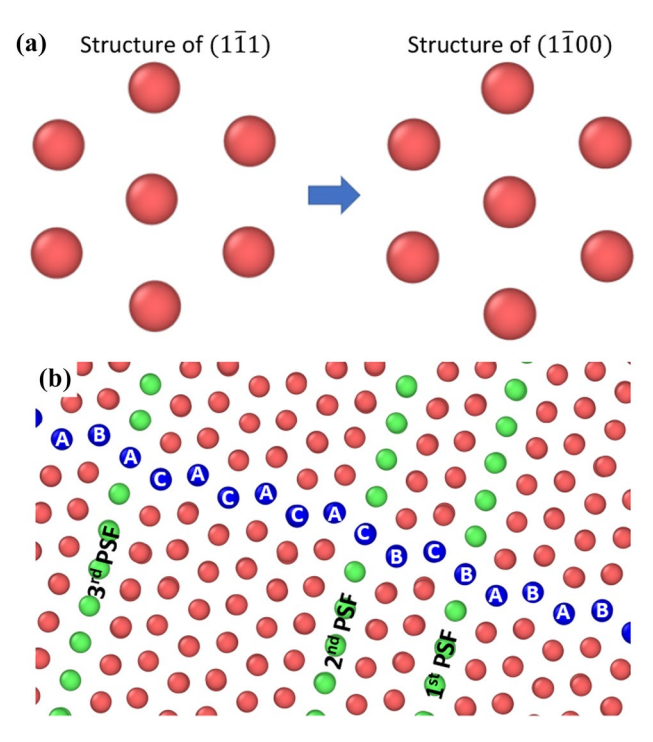


Figure 10 a Magnified views of the structure of the  $(1\overline{1}1)$  of FCC and the structure of  $(1\overline{1}00)$ , i.e., the prismatic plane of HCP. The viewing direction is along the normal of the preselected  $(1\overline{1}1)$ . The two planes have a very close similarity in structure and mutual transformation between these two planes is extremely easy, rendering the interfaces between them highly mobile. Only minor atomic shuffles are needed for the transformation. **b** Magnified view of the basal stacking faults (SFs) inside the HCP. The analysis of the stacking sequence indicates that these SFs are partial stacking faults (PSFs), i.e., only those atoms on every other basal plane are displaced by the formation of the SFs.

in dimensions. The major difference comes from the fact that the  $\{1\bar{1}00\}_{HCP}$  has a double-layered structure in the plane normal direction. This means that some atoms of the  $(1\bar{1}1)_{FCC}$  must shuffle along the plane normal so that the originally single-layered  $(1\bar{1}1)_{FCC}$  becomes a double-layered  $\{1\bar{1}00\}_{HCP}$ .

The shuffling-dominated lattice transformation in Fig. 10a is the root cause of the basal SFs in the HCP phase shown in Figs. 2, 3, 4, 5, 6, 7, 8. These SFs are called "partial stacking faults (PSFs)" and a magnified view of an example PSF is shown in Fig. 10b. The concept of PSF was first proposed by Song and Gray [29] to distinguish them from conventional SFs such as  $I_1$  type (SFs produced by Frank partials on the close-packed planes [30–32]) and  $I_2$  type (SFs produced by the glide of Shockley partials [33]). PSFs are typically observed inside  $\{10\overline{12}\}\langle10\overline{11}\rangle$  and  $\{10\overline{11}\}\langle10\overline{12}\rangle$ 

twins in HCP structures that require quite large and complex shuffles [29, 34–38], but not in  $\{1122\}\langle 1123\rangle$ and  $\{11\overline{21}\}\langle11\overline{26}\rangle$  modes which only involve simple shuffles [39-42]. Song and Gray [29] conducted transmission electron microscopy (TEM) observations on deformed HCP metals such as Ti and Zr and found high density basal SFs inside {1012}(1011) twins which is the most commonly observed twinning mode in HCP structures. These basal SFs presented anomalous diffraction contrast and were not associated with Shockley partial dislocations. Figure 10b shows the analysis of stacking sequence in the faulted HCP structure, and the meaning of "PSF" is clearly explained. Starting from the lower right, the stacking sequence in the perfect HCP is marked as "...BABAB...". When the first PSF is present, the stacking sequence changes to "BCBC." Thus, the positions of those atoms on the B layers are not changed when the SF is formed, and only those atoms on the A positions are displaced. This indicates that only atoms on every other basal plane or only 50% of atoms are displaced by the basal SFs, fundamentally different from SFs produced by Shockley partials and Frank partials that displace all the atoms by the Burgers vector of the partial dislocations. Similar analysis can be performed for the second and third PSFs and similar behavior can be clearly seen.

Song and Gray [29, 43, 44] attributed these basal SFs to atomic shuffles that are required in  $\{1012\}\langle 1011\rangle$ twinning. They also proposed that {1012}(1011) twinning was not mediated by twinning dislocations but rather by movements of a large number of atoms. Li and Ma [45] conducted atomistic simulations on {1012}(1011) twinning in magnesium and found that this twinning process was accomplished by the lattice transformation of  $(0002)_{parent} \rightarrow \{1100\}_{twin}$  and  $\{1100\}_{parent} \rightarrow (0002)_{twin}$ , i.e., the parent basal plane must be transformed into the twin prismatic plane and vice versa. Li and Zhang [46, 47] further proved that such lattice transformations exclude any possible shear along the  $\{10\overline{12}\}$  twinning plane because the structure of the {1012} twinning plane must be distorted and the requirement that the twinning plane of a twinning mode must not be distorted, i.e., maintain invariant in the classical twinning theory [11, 12] does not hold. Thus, such lattice transformations only involve atomic shuffles, rendering {1012} twin boundaries, mostly are  $(0002) \parallel \{\overline{1100}\}$  (i.e., B/P or P/B) type of interfaces, extremely mobile and reversible. Note that both FCC



and HCP are close-packed structures, and the structure of  $(1\bar{1}1)_{FCC}$  is exactly the same as the  $(0002)_{HCP}$ . Therefore, the lattice transformation in FCC  $\rightarrow$  HCP phase transition is essentially similar to the easy lattice transformation in  $\{10\bar{1}2\}\langle10\bar{1}1\rangle$  twinning. This analysis perfectly explains the formation of HCP phase at the GB, and why such a phase transformation generates a very mobile interface between the FCC and HCP, and thus facilitates GB migration via shear coupling. Disconnections were proposed on incoherent  $\{10\bar{1}2\}$  twin boundaries with B/P and/or P/B interfaces [48, 49], as well as STGBs [7, 8, 50, 51], but how the defined disconnections transform one lattice into the other was not considered in the disconnection model.

As the value of  $\theta$  increases to 12° and 14°, not only the top interface, but also the bottom interface between the FCC and HCP becomes mobile (Figs. 4, 5). To understand this behavior, we take the two interfaces when  $\theta$  = 12° and show their structures in Fig. 11. The structure of top interface is shown in Fig. 11a. Again, it can be seen that the top interface is composed of a series of small facets that are of (111)<sub>FCC</sub> || {1100}<sub>HCP</sub>. As analyzed above, such an interface has a high mobility in the FCC  $\rightarrow$  HCP phase transformation. In contrast, the bottom interface is composed of a series of short facets that are of {1101}<sub>HCP</sub> || (111)<sub>FCC</sub> (Fig. 11b). Hence, when the bottom interface is migrating upward, it transforms the {1101}<sub>HCP</sub> into the (111)<sub>grain2</sub>. The lattice transformation can be described as:

$$\{1\overline{1}01\}_{\text{HCP}} \rightarrow (1\overline{1}1)_{\text{FCC}}$$

This type of  $\{1\overline{1}01\}_{HCP} \parallel (1\overline{1}1)_{FCC}$  interfaces also has a finite mobility. As shown above, the structure of  $(\overline{111})_{FCC}$  is exactly the same as  $(0002)_{HCP}$  because both are close-packed planes. Thus, the bottom interface can be treated as  $\{1101\}_{HCP} \parallel (0002)_{HCP}$ . Immediately, this is exactly the {1101}-(0002) pair of corresponding planes in  $\{1011\}\langle 1012\rangle$  twinning mode, the socalled "compression twinning" in HCP metals with c/a ratios below  $\sqrt{3}$  [52]. In this twinning mode, the migration of a {1011} coherent twin boundary transforms the (0002) of parent into the {1011} of twin and vice versa. The lattice transformation between these two planes is shown in Fig. 12. We first preselect a group of ten atoms on the (111) of FCC (see Fig. 13), after the  $(111)_{FCC}$  is transformed to the  $\{1101\}_{HCP}$ , we compare the structures of these two planes. To accomplish this lattice transformation, two columns

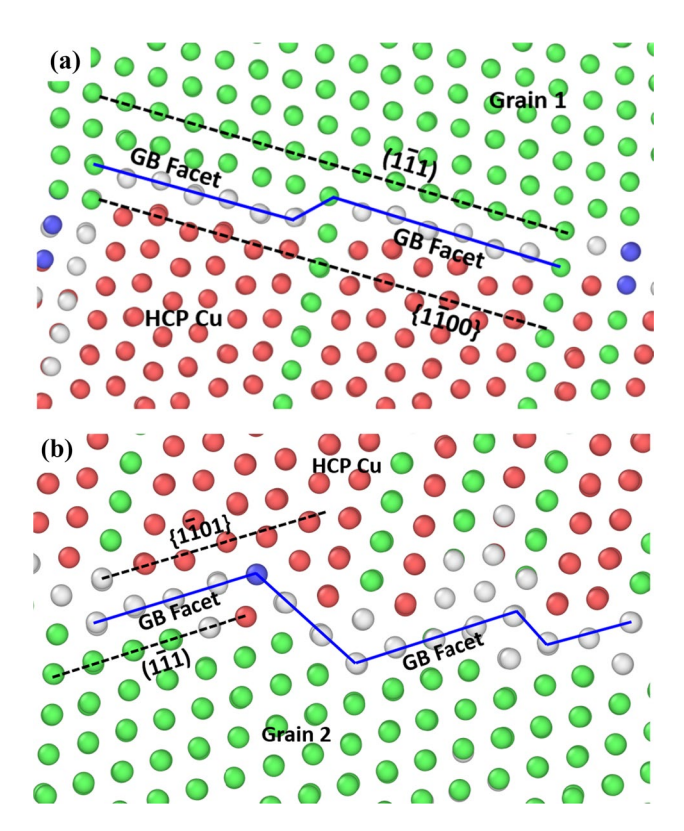


**Figure 11** Magnified views of the structure of the GBs in Fig. 14 ( $\theta$ =12°). **a** The top GB is composed of a series of small facets (the white atoms) that are interfaces of  $(1\overline{1}1)_{FCC} \parallel \{1\overline{1}00\}_{HCP}$ . **b** The bottom GB is composed of a series of small facets that are interfaces of  $(1\overline{1}1)_{FCC} \parallel \{1\overline{1}01\}_{HCP}$ . This indicates that the  $\{1\overline{1}01\}_{HCP}$  is transformed into the  $(1\overline{1}1)_{FCC}$  of Grain 2 when the bottom GB is migrating upward.

of atoms of  $(\overline{111})_{FCC}$  need to shuffle along the [110] direction, with a magnitude about  $\frac{1}{2}a_0$  ( $a_0$  is the lattice parameter) which is fairly large. Along with other minor shuffles including the shuffles that make the single-layered (111)<sub>FCC</sub> into a double-layered  $\{1\overline{1}01\}_{HCP}$ , the  $(1\overline{1}1)_{FCC}$  can be transformed into the {1101}<sub>HCP</sub>. Because the magnitude of the shuffles involved in this lattice transformation is pretty large, the mobility of  $\{1101\}_{HCP} \parallel (111)_{FCC}$  interface, i.e., the bottom interface, is lower than that of the  $\{1100\}_{HCP} \parallel (111)_{FCC}$  interface, i.e., the top interface. The reason why the bottom interface becomes more mobile as  $\theta$  increases to 12° and 14° is because  $\psi$ , which is the angle between the invariant planes of Grain 2 and the HCP, decreases with increasing  $\theta$ , leading to a smaller magnitude of shear s and a better GB mobility. On the other hand, the HCP is a metastable phase and tends to shrink via the motion of the bottom interface to lower the system energy.



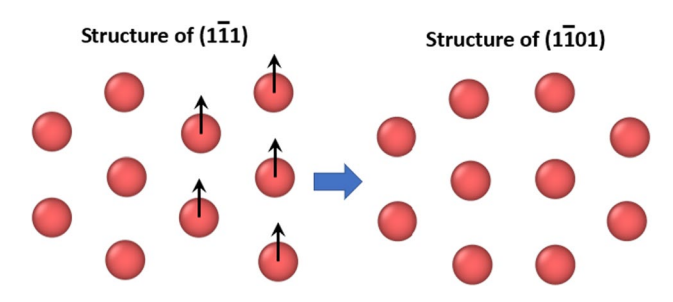


**Figure 12** Magnified views of the structure of  $(1\overline{1}1)$  of FCC and the structure of  $(1\overline{1}01)$  of HCP. If the two columns of atoms on  $(1\overline{1}1)$  shuffle upward (or downward) as indicated by the black arrows, together with other minor shuffles, the  $(1\overline{1}1)$  of FCC is transformed into the  $(1\overline{1}01)$  of HCP.

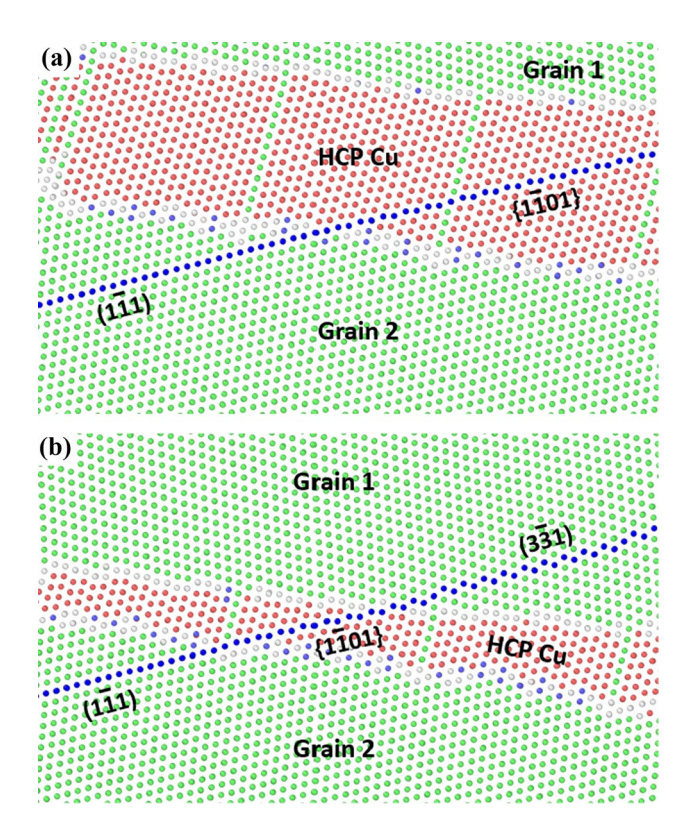


**Figure 13** Analysis of lattice correspondence in FCC $\rightarrow$ HCP $\rightarrow$ FCC phase transformations ( $\theta$ =14°). **a** A layer of atoms which contains a portion of (111) plane of the Grain 2, and a portion of the {1101} of the HCP are preselected and highlighted in blue. **b** The simulation is rewound to an earlier time step. It is clear that, as the HCP region moves upward, the (331) of the Grain 1 is transformed into the {1101} of the HCP, whereas the {1101} of the HCP is transformed into the (111) of Grain 2.

The  $\{1101\}_{HCP} \parallel (0002)_{HCP}$  type of interfaces or GBs with finite mobility has been observed in deformed HCP metals. Most recently, Liu et al. [53] conducted in situ TEM observations on c-axis compression of single crystal magnesium with submicron sizes. They found that the initial plastic deformation was dominated by glide of pyramidal or  $\langle c + a \rangle$  dislocations [54]. When the plastic strain reached about 36%, the single crystal suddenly evolved into polycrystal which was composed of multiple fine grains, accompanied by a large strain burst. The specimen abruptly pancaked with a total reduction in height over 60% without any signs of fracture. High-resolution TEM analyses revealed that many of the GBs between the fine, new grains were of {1101}<sub>HCP</sub> || (0002)<sub>HCP</sub> type, and they called this type of GBs "Py/B" boundaries. They also conducted atomistic simulations on the formation mechanism of this type of GBs and found that these GBs were indeed mobile. Kou et al. [55] performed in situ atomic-scale TEM observation of deformation of single crystal Ti. Formation of a new grain inside the specimen was revealed. The orientation relationship between the new grain and the matrix satisfies (0111) || (0002), i.e., the pyramidal plane of the new grain is parallel to the basal plane of the matrix. This orientation relationship is exactly the same as the observed  $\{1\overline{101}\}_{HCP} \parallel (1\overline{11})_{FCC}$  interface in our simulation.

In addition to the above-analyzed lattice transformations, i.e.,

 $(1\overline{11})_{\text{grain}1} \rightarrow (0002)_{\text{HCP}} \text{ and } (1\overline{11})_{\text{grain}1} \rightarrow \{1\overline{100}\}_{\text{HCP}},$ how the (111) of Grain 2 is transformed is still unknown. This is another close-packed plane of Grain 2 and it should correspond to a plane in the HCP and a plane in Grain 1 for the sequential phase transformations. To perform the lattice correspondence analysis, first we take a time step when  $\theta = 14^{\circ}$ . At this time step the HCP phase has traveled to near the top of Grain 1. Then we select a plane that contains a portion of the (111) plane of Grain 2 and a portion of the {1101} of the HCP region (Fig. 13a). Atoms on this plane are highlighted in blue. Then we rewind the simulation to an earlier time step (Fig. 13b). Immediately, it can now be seen that the corresponding plane in Grain 1 to the  $\{1101\}_{HCP}$  is (331), not one layer of (331) but two. Hence, as the HCP region is moving upward, two neighboring (331) planes are combined and transformed into the double-layered {1101}<sub>HCP</sub> mostly via atomic shuffling. While the bottom interface is also



moving upward, it transforms the  $\{1\overline{101}\}_{HCP}$  into the single-layered  $(1\overline{11})_{FCC}$  of Grain 2. The lattice correspondence can be described as:

$$2 \times (3\overline{3}1)_{grain1} \rightarrow 1 \times \{1\overline{1}01\}_{HCP} \rightarrow 1 \times (1\overline{1}1)_{grain2}$$

Without the formation of HCP along the GB, the lattice transformation would be  $2\times(3\overline{3}1)_{grain1}\to 1\times(1\overline{1}1)_{grain2}$ , which would be difficult to accomplish. It is now clear that, with the formation of HCP lattice, two neighboring  $(3\overline{3}1)$  planes of Grain 1, which have a pretty large interplanar spacing (~0.83 Å), becomes a double-layered  $\{1\overline{1}01\}_{HCP}$ . The double layers of a single  $\{1\overline{1}01\}_{HCP}$  has a reduced spacing (~0.35 Å), compared to that of two  $(3\overline{3}1)$  planes (Fig. 13b). Then the bottom interface transforms the double-layered  $\{1\overline{1}01\}_{HCP}$  into a single-layered  $(1\overline{1}1)_{FCC}$  of Grain 2. Therefore, the formation of HCP does facilitate shear coupling of the GBs.

Transitory phase transformations in twin boundary migration were observed in atomistic simulations of deformation of HCP Mg and Ti. Chen et al. [56] observed HCP  $\rightarrow$  BCC  $\rightarrow$  HCP<sub>twin</sub> at the beginning of {1012} twinning in Ti. The presence of BCC phase facilitated the lattice transformation for {1012} twinning in which the lattice transformation is  $\{1100\} \leftrightarrow (0002)$ , similar to the  $(111)_{FCC} \rightarrow \{1100\}_{HCP}$  in Fig. 9. After a {1012} twin was formed, an FCC phase formed and separated the matrix from the {1012} twin. Similar HCP → FCC → HCP<sub>twin</sub> transformations was also observed in Mg [57]. Formation of metastable FCC phase was observed in experiments as well. He et al. [58] conducted atomic-resolution in situ TEM observations of deformation of single crystal HCP rhenium (Re). They found that an FCC phase was formed along the {1012} TB which had a structure of {1100} || (0002). The FCC phase was formed at the intersections of the TB and the surfaces, accommodating the misfit strains produced by {1012} twinning.

### Lattice correspondence analysis in twinning at the GBs

As the value of  $\theta$  increases, the position of the top interface between Grain 1 and the HCP becomes increasingly close to the  $(\overline{111})_{FCC}$  of Grain 1 (Figs. 2, 3, 4, 5, 6). Further increase of  $\theta$  to about 18° and larger leads to the formation of a twin with respect to Grain 1 and the migration of the GB changes from upward

to downward (Figs. 7, 8). There are two reasons that drive this transition from HCP formation to twin formation. The first reason is that, as  $\theta$  increases, the obtuse angle between the (111) of Grain 1 and the (0002) of HCP (see Fig. 6b) becomes increasingly close to the angle between the second invariant planes of {111} twinning, i.e., the obtuse angle between the deflected blue  $(1\overline{11})$  planes (see Fig. 8c). At smaller values of  $\theta$  when an HCP phase forms, the top interface between Grain 1 and the HCP transforms the (111) of Grain 1 into the {1100} of HCP (see Fig. 6b). But as  $\theta$  increases and gets closer to the twin orientation, the formation of {1100}<sub>HCP</sub> is no longer favorable; instead, formation of (111)<sub>twin</sub> becomes favorable and can easily be accomplished by transformation of  $\{1\overline{1}00\}_{HCP}$  into  $(1\overline{1}1)_{FCC}$  (Fig. 10a). The second reason is that, as  $\theta$  increases to the range that favors twinning (Figs. 7, 8), the value of  $\psi$ , which is the angle between the (111) planes of Grain 2 and the twin, decreases with increasing  $\theta$ . The decrease in magnitude of shear s facilitates shear coupling of the GB between the twin and Grain 2.

Obviously, in the twin formation, the (111) of Grain 1 is transformed into the (111) of the twin and these two planes are the second invariant planes in {111} twinning of FCC metals. However, it is clear that the twin growth is fundamentally different from the classical twinning. Classically, a {111} twin grows by the glide of Shockley partial dislocations on consecutive {111} close-packed planes [12, 59–63]. After a twinning dislocation passes through, the twin boundary migrates by one layer of {111} toward the parent lattice. This way the twinning plane must always be on the {111}, i.e., the first invariant plane. The twin growth in Figs. 7 and 8 is, however, not mediated by Shockley partial dislocations because the twin boundary remains still during shear deformation. Instead, the twin growth is mediated by the motion of the GB via shear coupling. This raises a question as to how the lattice correspondence is accomplished in such a non-classical twinning behavior.

To conduct lattice correspondence in the twinning process in the case of  $\theta$  = 28° (similar analyses can be done for all other values of  $\theta$ ), a (111) plane of the twin is preselected at the final time step (Fig. 14a), and the atoms of the preselected (111) are colored in blue. Then the simulation is rewound to an earlier time step before the GB traverses through the



preselected atoms (Fig. 14b). It can now be seen that the corresponding plane in Grain 2 is an irrational plane that is composed of multiple small facets on the (111) planes of Grain 2. To better reveal the structure of the corresponding plane in Grain 2, a magnified view is shown in Fig. 15a. The size of the facets is less than 1.0 nm. Despite the facets, the average plane of the blue atoms is approximately parallel to the twin boundary. Figure 15b shows a time step when the GB is migrating downward and halfway through the preselected blue atoms. After the GB traverses through the blue atoms, the faceted blue plane is now a single-layered (111) plane of the twin.

Figures 14 and 15 clearly show that the twin growth is mediated by the migration of GB via shear coupling which is facilitated by the formation of a  $\{111\}$  twin along the original GB. The twin formation reduces the magnitude of shear s that favors shear coupling.

### Effect of stacking fault energy and twinnability of FCC metals

In the present work, phase transformation and twinning only occur in the STGBs with [110] tilt axis in Cu and Ni, but not in Al. It is well known that twinning is closely related to SF energy (SFE) of the closepacked {111} plane because a twin can be considered a pile of SFs produced by Shockley partial dislocation on consecutive {111} planes. Classically, FCC ↔ HCP transformation is mediated by Shockley partial dislocations on every other close-packed planes. Thus, both

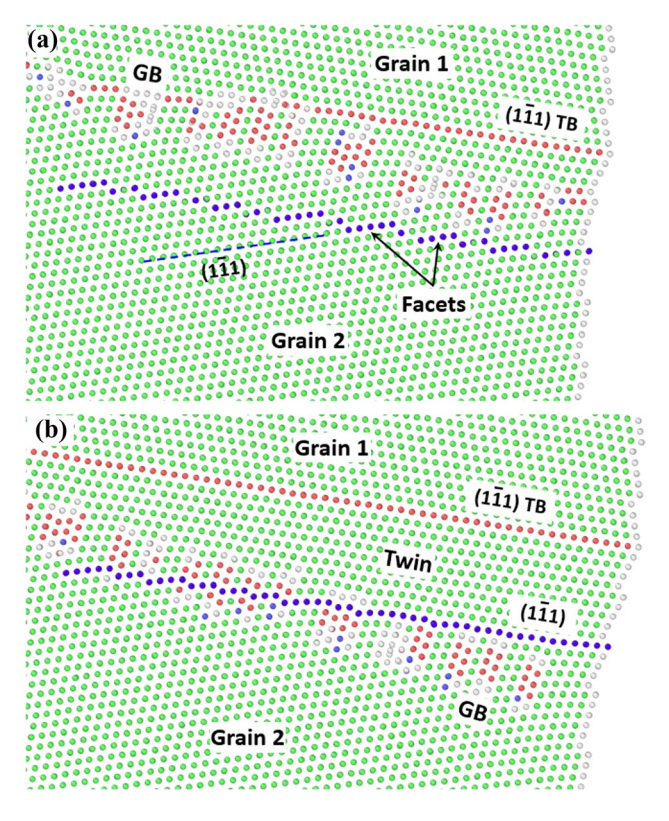


**Figure 15** Magnified views of lattice transformation during twin growth. **a** The blue atoms sit on a series of small segments that are on the  $(1\overline{1}1)$  of grain 2. (The trace is indicated by the dashed line.) **b** As the GB migrates downward and traverses through, the blue atoms are aligned to the  $(1\overline{1}1)$  plane of the twin.

twinning and phase transformation are related to SFE. In general, the lower the SFE, the easier for twinning and FCC  $\leftrightarrow$  HCP phase transformation to happen in

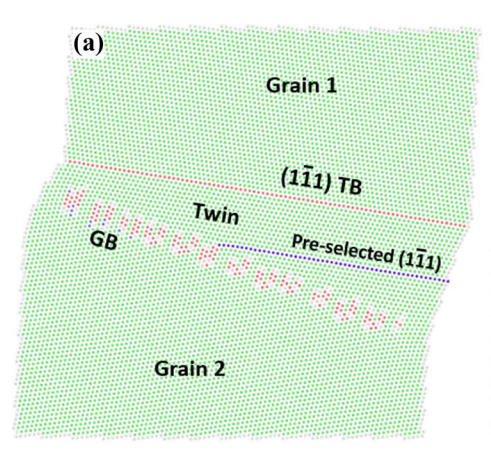
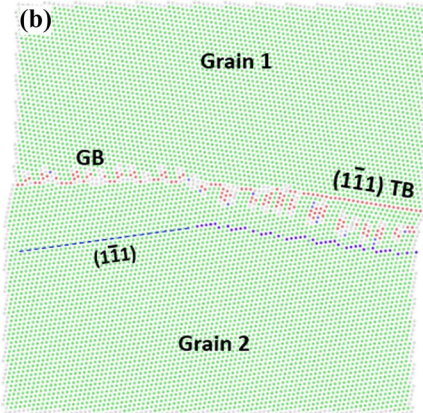


**Figure 14** Lattice correspondence analysis in twinning  $(\theta = 28^{\circ})$ . **a** A  $(1\overline{1}1)$  plane of the twin is preselected and highlighted in blue. **b** The simulation is rewound to an earlier time step before the GB traverses through the preselected blue atoms which are now



located on a series of  $(\overline{11})$  small facets of Grain 2. The average GB plane of the blue atoms is irrational but nearly parallel to the twin boundary. The trace of  $(\overline{11})$  of Grain 2 is denoted by the dashed blue line.



FCC metals. SFE can be obtained in atomistic or *ab initio* calculations by computing the gamma surfaces (aka generalized SFE or GSFE) [64]. Cahn et al. [1] computed the gamma surfaces for {100} and {110} planes and related the GSFE to the shear coupling modes in Cu observed in their simulations.

From the literature data of ab initio calculations, the SFEs are 40–43 mJ/m<sup>2</sup> for Cu, 110–133 mJ/m<sup>2</sup> for Ni and 130–160 mJ/m<sup>2</sup> for Al [65]. Thus, the FCC  $\rightarrow$  HCP phase transformation and twinning should be relatively easy to occur in Cu in the scenarios that such phase transformation and twinning facilitate GB shear coupling, as shown in our simulations. For Al, the SFE is relatively high, and no phase transformation and twinning are observed in Al (Fig. S3), and GBs only move by sliding. The SFE of Ni is also rather high, but phase transformation and twinning can readily occur at the GBs (Fig. S1 and S2). Hence, SFE may not be the sole factor that plays a role in the observed behavior. Considering that the stresses for twinning in FCC metals are not well correlated with SFEs, Tadmor and Bernstein [62] proposed the concept of twinnability for FCC metals. The twinnability  $\tau$  of an FCC metal was defined as:  $\tau = \frac{L}{\pi^4} \sqrt{\frac{\gamma_{\rm us}}{\gamma_{\rm ut}}}$ , where L is a material factor,  $\gamma_{\rm us}$ the unstable SFE (the energy barrier for shearing on a {111} along the twinning direction), and  $\gamma_{ut}$  the unstable twin fault energy (the energy barrier for subsequent shearing on the neighboring {111} along the twinning direction). According to their calculations, Al has the second lowest twinnability in FCC metals. This may explain the observed GB behavior in Al in our simulations.

The energy barrier to the  $(1\bar{1}1)_{FCC} \rightarrow \{1\bar{1}00\}_{HCP}$  (Figs. 9b and 10a) lattice transformation is computed in our simulation results. A group of seven atoms on the  $(1\bar{1}1)_{FCC}$  are preselected and the energy evolution of each atom is plotted. Figure 16a shows the result. In this case, atom 1 experiences the highest energy barrier, about 137 meV/atom. After the FCC  $\rightarrow$  HCP phase transformation, the energy of HCP is slightly higher than that of FCC by  $\sim$  10 meV/atom. The energy barrier to {111} twinning is shown in Fig. 16b. Similarly, the energy profile of seven atoms on the preselected (111) facet (Fig. 15a) are plotted. The highest energy barrier is about 129 meV/atom, experienced by atom 1. The two energy barriers are fairly close. Thus, both

can occur when the value of  $\theta$  is suitable for activating one of them.

### **Conclusions**

In this work, we investigate migration of STGBs with [110] tilt axis and ( $\overline{111}$ ) invariant plane in FCC metals under shear loading. GB shear coupling does not occur directly but is facilitated by FCC  $\rightarrow$  HCP phase transformation and {111} twinning. The following conclusions can be drawn:

- (1) For low values of θ, FCC → HCP phase transformation occurs along the original GB. One of the two interfaces between the FCC and HCP is highly mobile because it transforms the (111)<sub>FCC</sub> into the {1100}<sub>HCP</sub>. This lattice transformation is very similar to that of {1012} twinning mode which is the most popular mode in HCP metals. As θ increases, both interfaces are mobile and the HCP region moves by transforming the lattice of one grain into the other. The other interface transforms the {1101}<sub>HCP</sub> into the (111)<sub>FCC</sub> of the growing grain. This lattice transformation is very similar to one of the lattice correspondences in {1011} twinning mode in HCP metals
- (2) As θ further increases, the FCC → HCP phase transformation is no longer favorable, and {111} twinning occurs along the original GB. The GB migration switches its direction via shear coupling. The twin grows by GB shear coupling, rather than the glide of Shockley partial dislocations on the twin boundary
- (3) The lattice transformations involved the FCC → HCP phase transformation and {111} twinning on the GBs facilitates GB migration via shear coupling

### Acknowledgements

B.L. gratefully thanks the support from National Science Foundation, USA, under grant number CMMI-2016263 and 2032483.



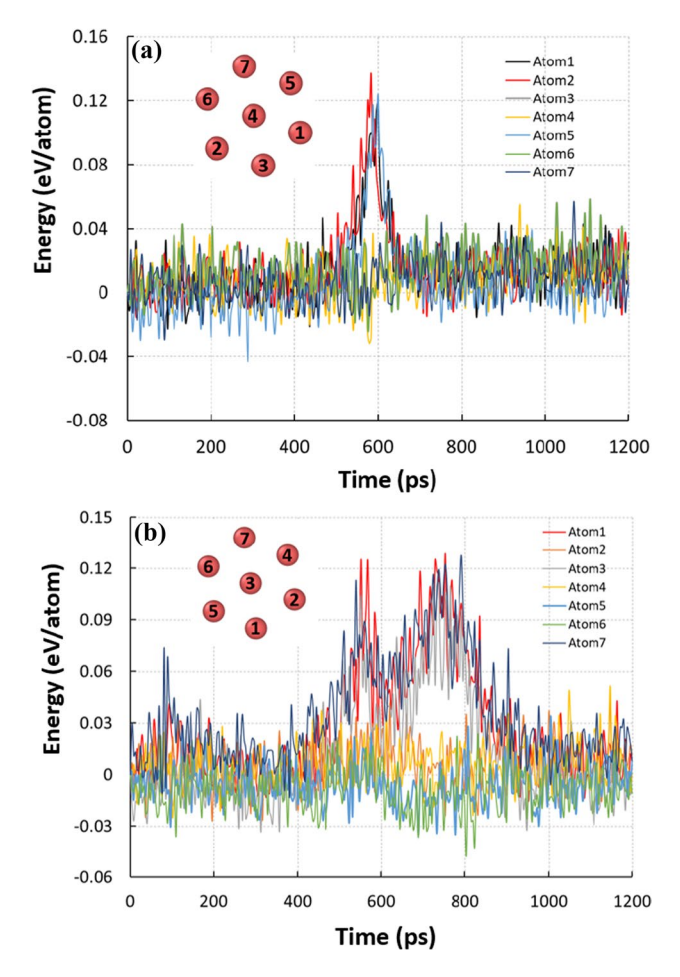


Figure 16 a Evolution of the potential energy of a selected group of seven atoms on the same  $(1\overline{1}1)$  plane of the top grain. The maximum value, i.e., energy barrier to the FCC $\rightarrow$ HCP phase transformation is about 137 meV/atom. **b** Evolution of the potential energy of a selected group of seven atoms on the same  $(1\overline{1}1)$  plane of the twin. The energy barrier to twin formation is about 129 meV/atom, which is comparable to that of FCC $\rightarrow$ HCP transformation.

### **Author contributions**

BL contributes to the design and execution of simulations, analyses, manuscript writing; KFC contributes to the simulations and analyses.

### Data and code availability

The original data of this work are available from the corresponding author (binl@iastate.edu) upon request.

### **Declarations**

**Conflict of interest** The authors declare no conflicts of interest or competing interests.

**Ethical approval** No human tissue is involved in this work.

**Supplementary Information** The online version contains supplementary material available at https://doi.org/10.1007/s10853-023-08863-z.

#### References

- [1] Cahn JW, Mishin Y, Suzuki A (2006) Coupling grain boundary motion to shear deformation. Acta Mater 54:4953-4975
- [2] Molodov DA, Gorkaya T, Gottstein G (2011) Dynamics of grain boundaries under applied mechanical stress. J Mater Sci 46:4318–4326. https://doi.org/10.1007/s10853-010-5233-6
- [3] Molodov DA, Gorkaya T, Gottstein G (2011) Migration of the Σ7 tilt grain boundary in Al under an applied external stress. Scr Mater 65:990–993
- [4] Fukutomi H, Kamijo T (1985) Grain boundary sliding-migration of aluminum (110) Σ11 {113} symmetric tilt coincidence grain boundary and its interpretation based on the motion of perfect DSC dislocations. Scr Metall 19:195–197
- [5] Cahn JW, Mishin Y, Suzuki A (2006) Duality of dislocation content of grain boundaries. Philos Mag 86:3965–3980
- [6] Caillard D, Mompiou F, Legros M (2009) Grain-boundary shear-migration coupling. II. Geometrical model for general boundaries. Acta Mater 57:2390–2402
- [7] Deng Y, Deng C (2017) Size and rate dependent grain boundary motion mediated by disconnection nucleation. Acta Mater 131:400–409
- [8] Han J, Thomas SL, Srolovitz DJ (2018) Grain-boundary kinetics: a unified approach. Prog Mater Sci 98:386–476
- [9] Molodov KD, Molodov DA (2018) Grain boundary mediated plasticity: on the evaluation of grain boundary migration-shear coupling. Acta Mater 153:336–353
- [10] Brandon DG (1966) The structure of high-angle grain boundaries. Acta Metall 14:1479–1484
- [11] Bilby BA, Crocker AG (1965) The theory of the crystallography of deformation twinning. Proc R Soc Lond Ser Math Phys Sci 288:240–255



- [12] Christian JW, Mahajan S (1995) Deformation twinning. Prog Mater Sci 39:1–157
- [13] Li B, Leung J (2021) Lattice transformation in grain boundary migration via shear coupling and transition to sliding in face-centered-cubic copper. Acta Mater 215:117127
- [14] Homer ER, Foiles SM, Holm EA, Olmsted DL (2013) Phenomenology of shear-coupled grain boundary motion in symmetric tilt and general grain boundaries. Acta Mater 61:1048–1060
- [15] Wan L, Wang S (2009) Shear response of the  $\Sigma 11$ ,  $\langle 110 \rangle$  {131} symmetric tilt grain boundary studied by molecular dynamics. Model Simul Mater Sci Eng 17:045008
- [16] Wan L, Wang S (2010) Shear response of the  $\Sigma 9 \langle 110 \rangle$  {221} symmetric tilt grain boundary in fcc metals studied by atomistic simulation methods. Phys Rev B 82:214112
- [17] Daw MS, Baskes MI (1983) Semiempirical, quantum mechanical calculation of hydrogen embrittlement in metals. Phys Rev Lett 50:1285–1288
- [18] Daw MS, Baskes MI (1984) Embedded-atom method: derivation and application to impurities, surfaces, and other defects in metals. Phys Rev B 29:6443–6453
- [19] Mishin Y, Mehl MJ, Papaconstantopoulos DA et al (2001) Structural stability and lattice defects in copper: ab initio, tight-binding, and embedded-atom calculations. Phys Rev B 63:224106
- [20] Mishin Y, Farkas D, Mehl MJ, Papaconstantopoulos DA (1999) Interatomic potentials for monoatomic metals from experimental data and *ab initio* calculations. Phys Rev B 59:3393–3407
- [21] Hoover WG (1985) Canonical dynamics: equilibrium phase-space distributions. Phys Rev A 31:1695–1697
- [22] Nosé S (1984) A unified formulation of the constant temperature molecular dynamics methods. J Chem Phys 81:511–519
- [23] Plimpton S (1995) Fast parallel algorithms for short-range molecular dynamics. J Comput Phys 117:1–19
- [24] Stukowski A (2010) Visualization and analysis of atomistic simulation data with OVITO-the open visualization tool. Model Simul Mater Sci Eng 18:015012
- [25] Honeycutt JD, Andersen HC (1987) Molecular dynamics study of melting and freezing of small Lennard-Jones clusters. J Phys Chem 91:4950–4963
- [26] Rittner JD, Seidman DN, Merkle KL (1996) Grain-boundary dissociation by the emission of stacking faults. Phys Rev B 53:R4241–R4244
- [27] Christian JW (2002) The theory of transformations in metals and alloys. Newnes
- [28] Niewczas M (2010) Lattice correspondence during twinning in hexagonal close-packed crystals. Acta Mater 58:5848–5857

- [29] Song SG, Gray GT (1995) Transmission electron microscopy examination and analysis of an anomalous stacking fault in h.c.p. metals. Philos Mag A 71:263–274
- [30] Zinkle SJ, Seitzman LE, Wolfer WG (1987) I. Energy calculations for pure metals. Philos Mag A 55:111–125
- [31] Varvenne C, Mackain O, Clouet E (2014) Vacancy clustering in zirconium: an atomic-scale study. Acta Mater 78:65–77
- [32] Wu XL, Li B, Ma E (2007) Vacancy clusters in ultrafine grained Al by severe plastic deformation. Appl Phys Lett 91:141908
- [33] Hirth JP, Lothe J (1983) Theory of dislocations, 2nd edn. Krieger Publishing Company
- [34] Zhang XY, Li B, Liu Q (2015) Non-equilibrium basal stacking faults in hexagonal close-packed metals. Acta Mater 90:140–150
- [35] Li B, Sun Q, Zhang XY (2021) Lattice correspondence analysis on the formation mechanism for partial stacking faults in hexagonal close-packed metals. Comput Mater Sci 198:110684
- [36] Sun Q, Zhang Q, Li B et al (2017) Non-dislocation-mediated basal stacking faults inside {1011} 〈1012〉 twins. Scr Mater 141:85–88
- [37] Zhou B, Sui M (2019) High density stacking faults of {1011} compression twin in magnesium alloys. J Mater Sci Technol 35:2263–2268
- [38] Li B, Ma E (2009) Zonal dislocations mediating twinning in magnesium. Acta Mater 57:1734–1743
- [39] Minonishi Y, Ishioka S, Koiwa M, Mobozumi S (1982) The structure of {1121} twin boundaries in H.C.P. crystals. Phys Status Solidi A 71:253–258
- [40] Li B, El Kadiri H, Horstemeyer MF (2012) Extended zonal dislocations mediating twinning in titanium. Philos Mag 92:1006–1022
- [41] Li J, Sui M, Li B (2021) A half-shear-half-shuffle mechanism and the single-layer twinning dislocation for  $\{1122\}$   $\langle 1123 \rangle$  mode in hexagonal close-packed titanium. Acta Mater 216:117150
- [42] Chen P, Ombogo J, Li B (2020) Dislocation ↔ twin transmutations during interaction between prismatic slip and {1011} twin in magnesium. Acta Mater 186:291–307
- [43] Song SG, Gray GT III (1995) Structural interpretation of the nucleation and growth of deformation twins in Zr and Ti—I. Application of the coincidence site lattice (CSL) theory to twinning problems in h.c.p. structures. Acta Metall Mater 43:2325–2337
- [44] Song SG, Gray GT III (1995) Structural interpretation of the nucleation and growth of deformation twins in Zr and Ti—II. Tem study of twin morphology and defect reactions during twinning. Acta Metall Mater 43:2339–2350



- [45] Li B, Ma E (2009) Atomic shuffling dominated mechanism for deformation twinning in magnesium. Phys Rev Lett 103:035503
- [46] Li B, Zhang XY (2016) Twinning with zero twinning shear. Scr Mater 125:73–79
- [47] Li B, Zhang XY (2014) Global strain generated by shuffling-dominated twinning. Scr Mater 71:45–48
- [48] Hirth JP, Wang J, Tomé CN (2016) Disconnections and other defects associated with twin interfaces. Prog Mater Sci 83:417–471
- [49] Dang K, Wang S, Gong M et al (2020) Formation and stability of long basal-prismatic facets in Mg. Acta Mater 185:119–128
- [50] Chen K, Han J, Thomas SL, Srolovitz DJ (2019) Grain boundary shear coupling is not a grain boundary property. Acta Mater 167:241–247
- [51] Combe N, Mompiou F, Legros M (2016) Disconnections kinks and competing modes in shear-coupled grain boundary migration. Phys Rev B 93:024109
- [52] Yoo MH (1981) Slip, twinning, and fracture in hexagonal close-packed metals. Metall Trans A 12:409–418
- [53] Liu B-Y, Zhang Z, Liu F et al (2022) Rejuvenation of plasticity via deformation graining in magnesium. Nat Commun 13:1060
- [54] Liu B-Y, Liu F, Yang N et al (2019) Large plasticity in magnesium mediated by pyramidal dislocations. Science 365:73–75
- [55] Kou Z, Yang Y, Yang L et al (2019) In situ atomic-scale observation of a novel lattice reorienting process in pure Ti. Scr Mater 166:144–148
- [56] Chen P, Wang F, Li B (2019) Transitory phase transformations during 1012 twinning in titanium. Acta Mater 171:65–78
- [57] Chen P, Wang F, Li B (2019) Misfit strain induced phase transformation at a basal/prismatic twin

- boundary in deformation of magnesium. Comput Mater Sci 164:186–194
- [58] He Y, Li B, Wang C, Mao SX (2020) Direct observation of dual-step twinning nucleation in hexagonal close-packed crystals. Nat Commun 11:2483
- [59] Mahajan S, Chin GY (1973) Formation of deformation twins in f.c.c. crystals. Acta Metall 21:1353–1363
- [60] Li B, Cao BY, Ramesh KT, Ma E (2009) A nucleation mechanism of deformation twins in pure aluminum. Acta Mater 57:4500–4507
- [61] Kibey S, Liu JB, Johnson DD, Sehitoglu H (2007) Predicting twinning stress in fcc metals: linking twin-energy pathways to twin nucleation. Acta Mater 55:6843–6851
- [62] Tadmor EB, Bernstein N (2004) A first-principles measure for the twinnability of FCC metals. J Mech Phys Solids 52:2507–2519
- [63] Li BQ, Sui ML, Li B et al (2009) Reversible twinning in pure aluminum. Phys Rev Lett 102:205504
- [64] Vítek V (1968) Intrinsic stacking faults in body-centred cubic crystals. Philos Mag 18:773–786
- [65] Rodney D, Ventelon L, Clouet E et al (2017) Ab initio modeling of dislocation core properties in metals and semiconductors. Acta Mater 124:633–659

**Publisher's Note** Springer Nature remains neutral with regard to jurisdictional claims in published maps and institutional affiliations.

Springer Nature or its licensor (e.g. a society or other partner) holds exclusive rights to this article under a publishing agreement with the author(s) or other rightsholder(s); author self-archiving of the accepted manuscript version of this article is solely governed by the terms of such publishing agreement and applicable law.

